Monthly Notices
of the
ROYAL ASTRONOMICAL SOCIETY

MNRAS **430,** 924–933 (2013) doi:10.1093/mnras/sts608

The WiggleZ Dark Energy Survey: measuring the cosmic growth rate with the two-point galaxy correlation function

Carlos Contreras,[1]⋆ Chris Blake,[1] Gregory B. Poole,[1] Felipe Marin,[1] Sarah Brough,[2] Matthew Colless,[2] Warrick Couch,[1] Scott Croom,[3] Darren Croton,[1] Tamara M. Davis,[4] Michael J. Drinkwater,[4] Karl Forster,[5] David Gilbank,[6] Mike Gladders,[7] Karl Glazebrook,[1] Ben Jelliffe,[3] Russell J. Jurek,[8] I-hui Li,[1] Barry Madore,[9] D. Christopher Martin,[5] Kevin Pimbblet,[10] Michael Pracy,[3] Rob Sharp,[2,11] Emily Wisnioski,[1] David Woods,[12] Ted K. Wyder[5] and H. K. C. Yee[13]

[1]*Centre for Astrophysics & Supercomputing, Swinburne University of Technology, PO Box 218, Hawthorn, VIC 3122, Australia*
[2]*Australian Astronomical Observatory, PO Box 296, Epping, NSW 1710, Australia*
[3]*Sydney Institute for Astronomy, School of Physics, University of Sydney, NSW 2006, Australia*
[4]*School of Mathematics and Physics, University of Queensland, Brisbane, QLD 4072, Australia*
[5]*California Institute of Technology, MC 278-17, 1200 East California Boulevard, Pasadena, CA 91125, USA*
[6]*South African Astronomical Observatory, PO Box 9, Observatory, 7935, South Africa*
[7]*Department of Astronomy and Astrophysics, University of Chicago, 5640 South Ellis Avenue, Chicago, IL 60637, USA*
[8]*Australia Telescope National Facility, CSIRO, Epping, NSW 1710, Australia*
[9]*Observatories of the Carnegie Institute of Washington, 813 Santa Barbara St., Pasadena, CA 91101, USA*
[10]*School of Physics, Monash University, Clayton, VIC 3800, Australia*
[11]*Research School of Astronomy & Astrophysics, Australian National University, Weston Creek, ACT 2611, Australia*
[12]*Department of Physics & Astronomy, University of British Columbia, 6224 Agricultural Road, Vancouver, BC V6T 1Z1, Canada*
[13]*Department of Astronomy and Astrophysics, University of Toronto, 50 St. George Street, Toronto, ON M5S 3H4, Canada*

Accepted 2012 December 12. Received 2012 December 11; in original form 2011 December 18

ABSTRACT

The growth history of large-scale structure in the Universe is a powerful probe of the cosmological model, including the nature of dark energy. We study the growth rate of cosmic structure to redshift $z = 0.9$ using more than 162 000 galaxy redshifts from the WiggleZ Dark Energy Survey. We divide the data into four redshift slices with effective redshifts $z =$ [0.2, 0.4, 0.6, 0.76] and in each of the samples measure and model the two-point galaxy correlation function in parallel and transverse directions to the line of sight. After simultaneously fitting for the galaxy bias factor we recover values for the cosmic growth rate which are consistent with our assumed Λcold dark matter (ΛCDM) input cosmological model, with an accuracy of around 20 per cent in each redshift slice. We investigate the sensitivity of our results to the details of the assumed model and the range of physical scales fitted, making close comparison with a set of *N*-body simulations for calibration. Our measurements are consistent with an independent power-spectrum analysis of a similar data set, demonstrating that the results are not driven by systematic errors. We determine the pairwise velocity dispersion of the sample in a non-parametric manner, showing that it systematically increases with decreasing redshift, and investigate the Alcock–Paczynski effects of changing the assumed fiducial model on the results. Our techniques should prove useful for current and future galaxy surveys mapping the growth rate of structure using the two-dimensional correlation function.

Key words: surveys – cosmological parameters – large-scale structure of Universe.

1 INTRODUCTION

The clustering pattern of galaxies, which is driven by the competing forces of gravitational attraction and universal cosmic expansion,

⋆E-mail: ccontrer@astro.swin.edu.au

is one of the most important probes of the cosmological model. In particular, measurements of the growth rate of cosmic structure, inferred from the patterns imprinted in the galaxy clustering distribution, can potentially distinguish between the increasing number of alternative theories of gravity which currently compete with General Relativity to explain the observed acceleration of the universal expansion without the need for an exotic component like Dark Energy (see Tsujikawa 2010, for a review). In general, the cosmic growth rate will evolve differently in these models, even if they have the same expansion history, allowing constraints to be placed on different theories of gravity (Linder & Jenkins 2003; Linder & Cahn 2007; Guzzo et al. 2008; Wang 2008).

It has long been known in standard gravity that the growth rate $f = \mathrm{d}\ln D/\mathrm{d}\ln a$ (in terms of the linear growth factor D and cosmic scale factor a) is well-approximated by $f(z) \approx \Omega_{\rm m}(z)^{0.6}$, where $\Omega_{\rm m}(z)$ is the matter density relative to critical density at redshift z (Peebles 1980). More recent theoretical investigations (Linder & Cahn 2007) have generalized this equation to a phenomenological relation

$$f(z) = \Omega_{\rm m}(z)^{\gamma} \quad (1)$$

where the parameter γ, the 'gravitational growth index', will take on different values depending on the considered theory of gravity, where $\gamma \approx 0.55$ for General Relativity in a Universe dominated by a cosmological constant Λ. In this study we test the self-consistency of the Λcold dark matter (ΛCDM) cosmological model on large scales by measuring the growth rate from a galaxy survey assuming a fiducial ΛCDM model and comparing these measurements with the predicted values.

A powerful technique for determining the growth rate is to measure and model redshift–space distortions imprinted in the two-point galaxy correlation function [hereafter $\xi_s(\sigma, \pi)$] of a galaxy redshift survey, where the two dimensions (σ, π) correspond to galaxy pair separations transverse and parallel to the line of sight. This is possible because the bulk flows of matter produced by large-scale structure formation leave a pattern of correlated peculiar velocities in the redshifts measured by galaxy surveys, introducing a characteristic distortion into the shape of the measured $\xi_s(\sigma, \pi)$.

The models used to fit the distorted pattern present in $\xi_s(\sigma, \pi)$ have their origins in the works of Kaiser (1987) and Hamilton (1992). The principal ingredients which make up these models are as follows

(i) The underlying real–space correlation function ($\xi_{\rm r}$), which describes the clustering of galaxies in the absence of redshift–space distortions. This function cannot be measured directly from real observations due to galaxy peculiar velocities, but can be modelled from theory or simulations.

(ii) A prescription for the large-scale linear distortion of the redshift–space correlation function due to galaxy bulk flows.

(iii) A function for the galaxy pairwise velocity distribution, $F(v)$, which represents non-linear effects in the velocity field resulting from small-scale interactions between galaxies and their surroundings. An example of these effects is the characteristic spike known as the 'finger-of-god' observed in $\xi_s(\sigma, \pi)$ at small tangential separations ($\sigma < 4\,h^{-1}$ Mpc), due to the virialized motions of galaxies in dark matter haloes.

(iv) A prescription for the bias with which galaxies trace the underlying matter density field.

Various approaches have been used in the literature for modelling these different components. In the simplest version of the model a power law is assumed for $\xi_{\rm r}$ on small scales, an exponential function for $F(v)$, and galaxies are assumed to trace the matter-density field with linear bias on large scales. This simple model has been applied to analyses many galaxy surveys including recent large spectroscopic surveys such as the 2-degree Field Galaxy Redshift Survey (2dFGRS; Colless et al. 2001) and the Sloan Digital Sky Survey (SDSS; York et al. 2000).

The 2dFGRS spans an area $\approx$1500 deg^2 mainly located in two regions of sky. Hawkins et al. (2003) used 166 000 2dFGRS galaxies in the redshift range $z = [0.0, 0.2]$ to measure $\xi_s(\sigma, \pi)$ up to separations of $30\,h^{-1}$ Mpc, constraining the growth rate with an accuracy of approximately 10 per cent at an effective redshift $z = 0.15$. The SDSS Luminous Red Galaxy (LRG) sample contains more than 75 000 objects in the more extended redshift range $z = [0.15, 0.47]$ spanning a volume bigger than $1\,h^{-3}$ Gpc^3. Its correlation function allows a measurement of f at an effective redshift of $z = 0.35$ (Okumura et al. 2008; Cabré & Gaztañaga 2009; Samushia, Percival & Raccanelli 2012). Noisier measurements of the growth rate have also been determined from higher-redshift surveys such as the VIMOS VLT Deep Survey (VVDS) at redshift $\approx$0.8 (Guzzo et al. 2008).

Other analyses of redshift–space distortions in the galaxy distribution, involving a wider range of cosmological parameters, include: the studies of Percival et al. (2004) who model the redshift–space distortions of the 2dFGRS by expanding its density field in spherical harmonics; Tegmark et al. (2006) who measure galaxy power spectra from SDSS LRGs at $z \sim 0.3$ and fit for a large set of cosmological parameters; and da Angela et al. (2008) who use QSO catalogues from the 2QZ and 2SLAQ surveys to compute and model $\xi_s(\sigma, \pi)$ for $z \sim 1.5$. These studies generally found agreement between the measurements and the predictions of the prevailing ΛCDM cosmological model.

Although galaxy redshift surveys currently provide the most accurate means of measuring the cosmic growth history, other methods are also being actively developed to extract this information. These include studies of the luminosity function of X-ray clusters and their physical properties such as gas mass fraction (Rapetti et al. 2009), measurements of bulk flows in the local neighbourhood (Abate & Lahav 2008; Watkins, Feldman & Hudson 2009; Nusser & Davis 2011) and weak lensing distortions mapped in large, high-quality photometric imaging surveys (Heavens, Kitching & Verde 2007; Bernstein 2009).

In this study we analyse redshift–space distortions in the two-point correlation function of the WiggleZ Dark Energy Survey (hereafter WiggleZ; Drinkwater et al. (2010)). This is a new high-redshift survey which has observed more than 200 000 galaxy redshifts over $\sim$1000 deg^2 of sky in the redshift range $z < 1$. The availability of the WiggleZ data enables accurate cosmological measurements to be carried out for the first time in the high-redshift ($z > 0.4$) Universe, the epoch at which the Universe apparently started its accelerating expansion. WiggleZ galaxies are selected as star-forming (blue) galaxies by photometric criteria (Blake et al. 2010; Drinkwater et al. 2010), in contrast to previous surveys which targeted LRGs, and therefore also allow us to investigate if the cosmological conclusions depend on the type of galaxy used to trace large-scale structure.

The growth rate has been measured from the WiggleZ data set by Blake et al. (2011a) using a power-spectrum analysis. In this study we carry out a correlation-function analysis of a similar data set. There is a strong motivation for performing both analyses. Cosmological measurements from large, modern galaxy surveys are limited not by statistical errors but by systematic errors, generally arising from modelling non-linear physics in addition to technical concerns such as determining the data covariance matrix in a sufficiently

robust and accurate manner. Systematics imprint themselves quite differently into analyses in configuration space and Fourier space. For example, a correlation-function analysis is more effective at separating processes which occur at different spatial scales (for example shot noise owing to the discreteness with which galaxies trace dark matter haloes is important at all scales in a power-spectrum measurement but only at small scales in the corresponding correlation function). Moreover, power-spectrum measurements are much more sensitive to how accurately the selection function of the survey can be quantified, which is a major issue of concern for a survey such as WiggleZ with relatively low redshift completeness (Blake et al. 2009). However, modelling of quasi-linear scales becomes more robust in a power-spectrum analysis, where linear theory can be more confidently applied across a range of values of wavenumber k (whereas structure with a given separation in configuration space depends on a set of underlying modes with a significant range of values of k). In general, the consistency of the power-spectrum and correlation-function analysis approaches is important to check, and would increase confidence in the robustness of the results against systematic error.

We have investigated in detail the modelling of redshift–space distortions in the correlation function in a companion paper (Contreras et al. 2013) using dark matter and halo catalogues from an N-body simulation. These results are important for our current study and we summarize them here.

(i) The commonly used power-law model for the real–space correlation function produces a poor fit to the clustering pattern and introduces considerable systematic errors in a growth rate measurement based on a large sample of galaxies. We considered two alternative models for the real–space correlation function, which are able to recover the growth rate with minimal systematic error.

(ii) We introduced a technique which permits a non-parametric determination of the galaxy pairwise velocity distribution from a 2D correlation function. We used this method to measure the pairwise velocity dispersion and check the consistency of the assumed functional form.

(iii) We explored the sensitivity of the results to the range of scales included in the fit, in particular considering different cuts for the minimum transverse scale fitted, $\sigma_{\rm min}$.

Our study of the growth rate in the WiggleZ correlation function is structured as follows: in Section 2 we describe our data and the measurements of $\xi_s(\sigma, \pi)$, and in Section 3 we summarize the models fitted. In Section 4 we determine the best-fitting model parameters and errors, comparing these measurements to the theoretical predictions of the ΛCDM cosmology using standard gravity. We also make an initial investigation of the sensitivity of our results to the fiducial cosmological model via the Alcock–Paczynski distortion. In Section 5 we summarize and discuss the results.

2 WIGGLEZ SURVEY DATA AND CORRELATION-FUNCTION MEASUREMENTS

2.1 Data

The WiggleZ Dark Energy Survey is the latest in a series of large spectroscopic galaxy redshift surveys mapping out large-scale structure in the Universe. The survey, which was carried out between August 2006 and January 2011, obtained more than 200 000 galaxy redshifts in the range $0.1 < z < 1.0$ spread across several different equatorial regions of sky, which together constitute a survey area of 1000 deg^2 and span a volume of approximately 1 h^{-3} Gpc^3. The observations were carried out at the 3.9-m Anglo-Australian Telescope (AAT) using the AAOmega spectrograph. Individual galaxy spectra were redshifted by WiggleZ team members.

A key characteristic of the WiggleZ Survey is the target selection criteria (Blake et al. 2010; Drinkwater et al. 2010) which are based on a combination of ultra-violet photometry from the *Galaxy Evolution Explorer* (*GALEX*) satellite and optical imaging from the SDSS and 2nd Red Cluster Sequence (RCS2) survey (Yee et al. 2005). WiggleZ galaxies are star-forming (emission-line) galaxies, which are expected to avoid the densest regions of galaxy clusters where star formation is suppressed by mechanisms such as ram-pressure stripping of the gas content of the galaxies. Hence this WiggleZ data set should be less susceptible to the non-linear clustering effects found on small scales (such as 'fingers-of-god') compared to surveys targeting more luminous, highly biased galaxies.

In this study we analyse a total of 162 454 WiggleZ galaxy redshifts, which are selected from the [1,3,9,11,15,22]-h regions after minor cuts for redshift and survey contiguity. We sub-divide the sample into four redshift slices spanning redshifts of [0.1–0.3], [0.3–0.5], [0.5–0.7] and [0.7–0.9]. Table 1 shows the details of the catalogues we used. We calculate an effective redshift $z_{\rm eff} = [0.21, 0.39, 0.61, 0.76]$ for the measurement in each redshift slice by averaging the mean redshifts of the galaxy pairs included in our analysis at the separations of interest.

2.2 Random catalogues

The galaxy correlation function is measured by comparing the pair-count of the data set in separate bins to that of a random, unclustered set of galaxies possessing the same selection function as the data. We generated random WiggleZ data sets using the method discussed by Blake et al. (2010). This process models several effects including the variation of the *GALEX* target density with dust and exposure time, the incompleteness in the current redshift catalogue, the

Table 1. The number of galaxies used in our analysis, and the effective redshift of our measurement, by region and redshift slice. The effective redshift was measured by averaging the mean redshift of each galaxy pair [$z_{\rm m} = (z_1 + z_2)/2$] for all the galaxy pairs counted in our two-point correlation-function measurements. For the scales of interest (0–50 h^{-1} Mpc) we find no significant dependence of $z_{\rm eff}$ on the pair separation.

$z_{\rm slice}$/Field	$z_{\rm eff}$	01 h	03 h	09 h	11 h	15 h	22 h	
Z1 [0.1–0.3]	0.21	3058	2973	2671	4025	3578	5782	22 087
Z2 [0.3–0.5]	0.39	2983	3522	7438	9581	10 942	7728	42 194
Z3 [0.5–0.7]	0.61	5702	5982	11 294	13 964	17 928	8924	63 794
Z4 [0.7–0.9]	0.76	3518	4315	5189	7077	8943	5337	34 379
Total		15 261	16 792	26 592	34 647	41 391	27 771	162 454

variation of that incompleteness imprinted across each 2-degree field by constraints on the positioning of fibres and throughput variations with fibre position, and the dependence of the galaxy redshift distribution on optical magnitude. Random catalogues, each containing the same number of galaxies as the data, are generated by a Monte Carlo process.

2.3 Correlation-function measurement

In order to measure $\xi_s(\sigma, \pi)$ we first converted the redshifts and celestial coordinates of the galaxies into comoving (x, y, z) spatial co-ordinates assuming a fiducial flat ΛCDM cosmological model with $\Omega_m = 0.27$ (and $H_0 = 100\,h\,\mathrm{km\,s^{-1}\,Mpc^{-1}}$). We investigate the sensitivity of our results to the fiducial model in Section 4.6. We then computed the number of galaxy pairs in a series of (σ, π) bins, where π and σ are the pair separations parallel and transverse to the line of sight, respectively, where we re-define the line-of-sight direction for every pair of galaxies using the bisector of their subtended angle on the celestial sphere, in the same manner as Hamilton (1993). We repeated this process using 100 random galaxy catalogues, and finally employed the Landy & Szalay estimator for $\xi_s(\sigma, \pi)$ (Landy & Szalay 1993):

$$\xi(\sigma, \pi) = \frac{DD - 2DR + RR}{RR} \qquad (2)$$

where DD is the data–data pair count, DR is the data–random pair count and RR is the random–random pair count. We computed these quantities in square (σ, π) bins with side $3\,h^{-1}$ Mpc over the ranges $0 < \sigma < 30\,h^{-1}$ Mpc, $0 < \pi < 30\,h^{-1}$ Mpc. We do not use any additional weights for each data or random object, noting that in a sample with relatively low number density such as WiggleZ, weighting results in a negligible improvement to the error in the correlation function over the range of scales of interest. The fibre-collision corrections are not important for the scales analysed here, and are ameliorated by repeat observations of each patch of sky to build up the target density. We measured $\xi_s(\sigma, \pi)$ in each separate WiggleZ region and redshift slice, and optimally combined the measurements for common redshift slices using inverse-variance weighting (see below). Fig. 1 illustrates the combined correlation-function data for each of the four redshift slices.

2.4 Covariance matrix

We used a jack-knife procedure to measure the correlation-function variances and covariances between bins. This technique is implemented by sub-dividing the data set into N_{JK} equal volumes, then repeating the $\xi_s(\sigma, \pi)$ computation N_{JK} times excluding each of the subsets in turn. Using this procedure we obtain N_{JK} different,

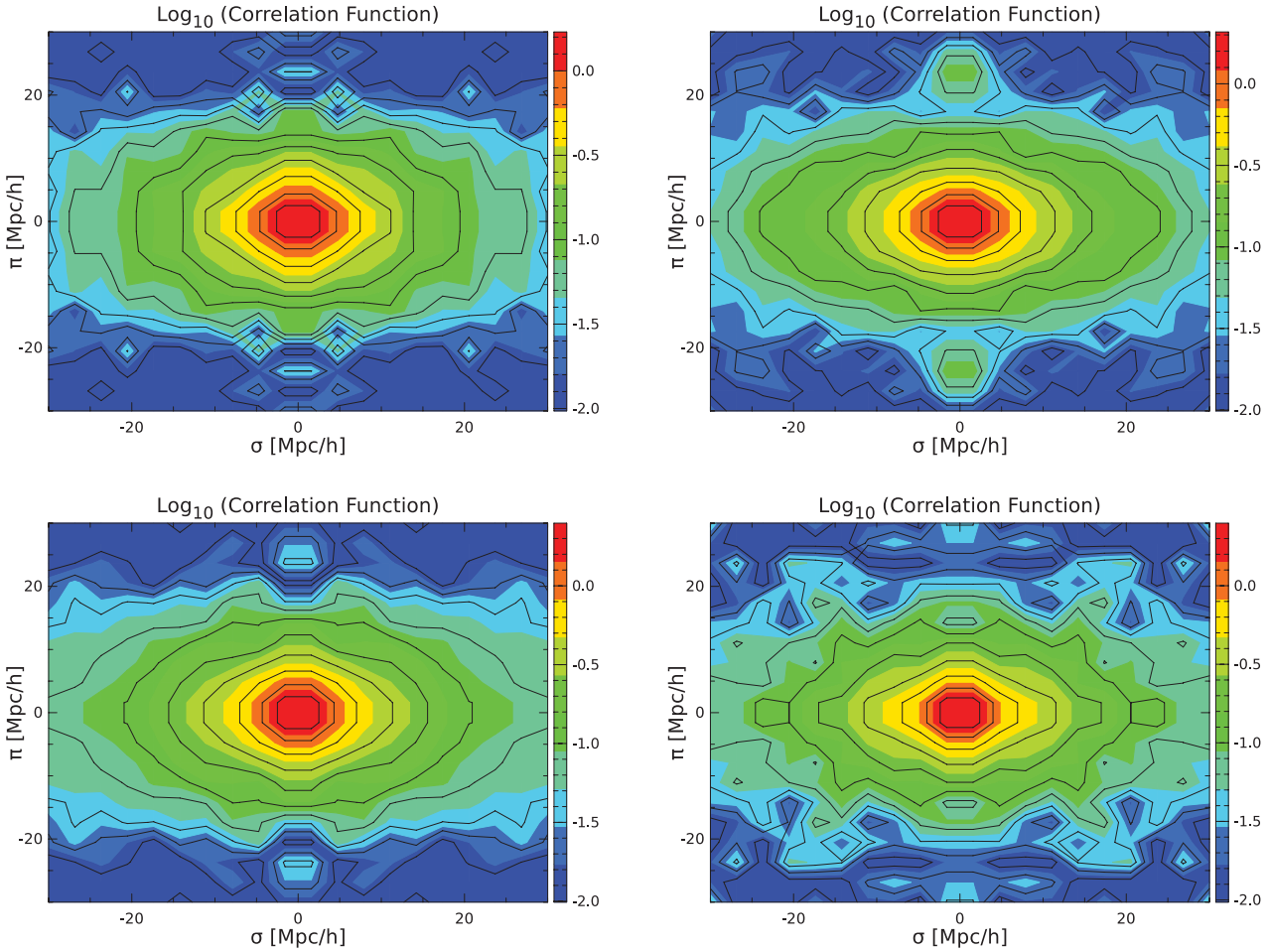

Figure 1. Measurements of the redshift–space correlation function for redshift slices 0.1–0.3 (top left), 0.3–0.5 (top right), 0.5–0.7 (bottom left) and 0.7–0.9 (bottom right), obtained by combining results in the different WiggleZ Survey regions with inverse-variance weighting. Only the top-right quadrant of data for each redshift is independent; the other three quadrants are mirrors of this first quadrant. Noticeable is the lack of 'fingers-of-god' prominent in similar measurements for LRGs, owing to the avoidance by WiggleZ galaxies of high-density regions.

correlated measurements of $\xi_s(\sigma, \pi)$. In order to compute the full covariance matrix between the bins we use the expression

$$C(\xi_i, \xi_j) = (N_{JK} - 1)(\langle \xi_i \xi_j \rangle - \langle \xi_i \rangle \langle \xi_j \rangle). \quad (3)$$

In our analysis we used $N_{JK} = 125$ for each individual survey region, choosing equal-volume sub-regions tiled in three dimensions, corresponding to a total $N_{JK} = 750$ for the combination of the six regions. We checked that our results were not sensitive to these choices. Excluding the diagonal elements, the correlation coefficients from the combined covariance matrices have consistently low average values 0.10 ± 0.10; 0.09 ± 0.08; 0.07 ± 0.08 and 0.03 ± 0.07 for the four redshift slices in ascending redshift order.

The combination of $\xi_s(\sigma, \pi)$ for the six sky regions for every redshift slice is produced using inverse-variance weighting:

$$\xi_i = \left(\sum_{k=1}^{6} \frac{\xi_{i,k}}{\sigma_{i,k}^2} \right) \left(\sum_{k=1}^{6} \frac{1}{\sigma_{i,k}^2} \right)^{-1} \quad (4)$$

for the ith bin, and the covariance matrices are combined as

$$C(\xi_i, \xi_j) = \left(\sum_{k=1}^{6} \frac{C(\xi_i, \xi_j)_k}{\sigma_{i,k}^2 \sigma_{j,k}^2} \right) \left(\sum_{k=1}^{6} \frac{1}{\sigma_{i,k}^2} \sum_{k=1}^{6} \frac{1}{\sigma_{j,k}^2} \right)^{-1} \quad (5)$$

for the ith and the jth bin of $\xi_s(\sigma, \pi)$. We determined the bin size ($3\,h^{-1}$ Mpc) of our measurement as a compromise between mapping the (σ, π) plane with high resolution, and the need to obtain an invertible covariance matrix. A smaller bin size would require a larger number of jack-knife sub-volumes to ensure a non-singular covariance matrix, resulting in smaller jack-knife regions which would be less independent on the scales of interest.

3 MODELS FOR THE 2D CORRELATION FUNCTION

The effect of linear redshift–space distortions on the power spectrum in Fourier space was described by Kaiser (1987):

$$P_s(k, \mu) = (1 + \beta \mu^2)^2 P_{\rm r}(k) \quad (6)$$

where P_s and $P_{\rm r}$ are the redshift–space and real–space galaxy power spectra at wavenumbers k, μ is the cosine of the angle of the Fourier mode to the line of sight, and $\beta = f/b$ quantifies the amplitude of redshift–space distortions in terms of the growth rate f and linear bias factor b. Hamilton (1992) provided the equivalent expression in configuration-space:

$$\xi_s'(\sigma, \pi) = \xi_0(r) P_0(\mu) + \xi_2(r) P_2(\mu) + \xi_4(r) P_4(\mu), \quad (7)$$

where P_ℓ are the Legendre polynomials and the correlation-function multipoles $\xi_\ell(r)$ are given by the general expressions:

$$\xi_0(r) = \left(1 + \frac{2\beta}{3} + \frac{\beta^2}{5} \right) \xi_{\rm r}(r) \quad (8)$$

$$\xi_2(r) = \left(\frac{4\beta}{3} + \frac{4\beta^2}{7} \right) \left[\xi_{\rm r}(r) - \dot{\xi}_{\rm r}(r) \right] \quad (9)$$

$$\xi_4(r) = \left(\frac{8\beta^2}{35} \right) \left[\xi_{\rm r}(r) + \frac{5}{2} \dot{\xi}_{\rm r}(r) - \frac{7}{2} \ddot{\xi}_{\rm r}(r) \right] \quad (10)$$

in terms of the integrals

$$\dot{\xi}_{\rm r}(r) = \frac{3}{r^3} \int_0^r \xi_{\rm r}(s) s^2 \, {\rm d}s \quad (11)$$

$$\ddot{\xi}_{\rm r}(r) = \frac{5}{r^5} \int_0^r \xi_{\rm r}(s) s^4 \, {\rm d}s. \quad (12)$$

In order to complete the model, the 2D correlation function including linear redshift–space distortions, $\xi_s'(\sigma, \pi)$, is then convolved with a function $F(v)$ representing a dispersion of pairwise velocities on small scales:

$$\xi_s(\sigma, \pi) = \int_{-\infty}^{\infty} \xi_s' \left(\sigma, \pi - \frac{v}{H(z) a(z)} \right) F(v) \, {\rm d}v \quad (13)$$

normalized such that $\int_{-\infty}^{\infty} F(v) \, {\rm d}v = 1$.

The most common approach in previous analyses of redshift–space distortions in the galaxy correlation function has been to use a power-law choice for $\xi_{\rm r}$ and an exponential 1D velocity distribution for $F(v)$ (Landy & Szalay 1998; Hawkins et al. 2003; Cabré & Gaztañaga 2009). In a companion paper (Contreras et al. 2013) we presented a detailed analysis of the systematic errors resulting from these assumptions, considering three different models for the underlying real–space correlation function $\xi_{\rm r}$:

(i) *Power-law model:* $\xi_{\rm r}(r) = (\frac{r}{r_0})^{-\gamma}$.

(ii) *CAMB model:* we use a real–space correlation function calculated numerically for a given set of cosmological parameters (motivated by analyses of the Cosmic Microwave Background radiation) using the CAMB software (Lewis, Challinor & Lasenby 2000) with the 7-year *Wilkinson Microwave Anisotropy Probe* (*WMAP*7) best-fitting cosmological parameters.

(iii) *Quadratic Correlation-Function (QCF) model:* we generalize the power-law function to an empirical real–space correlation with one further degree of freedom: $\xi_{\rm r}(r) = (\frac{r}{r_0})^{-\gamma + q \log_{10}(\frac{r}{r_0})}$. This form has more flexibility to describe the real–space correlation function than the other models. For $q = 0$ the QCF recovers the power law, while for $q \sim -0.5$ the QCF is similar to a CAMB correlation function.

We note two advantages of the QCF model. First it does not assume a particular set of cosmological parameters, and so represents a more flexible, model-independent approach that is able to reproduce the shape of the CAMB correlation function for a range of cosmological parameters. Secondly, the flexibility of the QCF model allows it to accommodate effects such as scale-dependent bias, which is expected to be important for massive haloes hosting LRGs.

In Contreras et al. (2013) we also considered a series of options for the shape of the pairwise velocity distribution function $F(v)$, introducing a parameter x which interpolates between exponential and Gaussian shapes for this function:

$$F(v) = x F(v)_{\rm e} + (1 - x) F(v)_{\rm g}. \quad (14)$$

The motivation for adding this parameter was to allow the data to determine which of the exponential or Gaussian distributions provided the best fit. We found that, when fitting to halo catalogues from dark matter simulations, the small-scale non-linear anisotropy in the clustering pattern favoured the exponential form, whilst if we excluded the small-scale part of the data by restricting the fitted range to $\sigma > \sigma_{\rm min}$ the choice of exponential or Gaussian was rendered unimportant. In our study of N-body simulations we were able to measure the shape of the pairwise velocity distribution directly, and the results were self-consistent with the best-fitting model for $F(v)$ when the CAMB or QCF models were used for the real–space correlation function. When the power-law model was used for $\xi_{\rm r}(r)$

instead, we found systematically higher values for the pairwise velocity dispersion. This result provided more evidence that using an accurate model for the real–space correlation function yielded constraints for all the fitted variables with lower systematic error.

We reformulated the problem of obtaining the pairwise velocity distribution by the process of fitting a non-parametric stepwise function instead of an exponential or Gaussian profile. We introduced a fast technique to do this (Contreras et al. 2013, appendix A). The results for the pairwise velocity dispersion measured as a stepwise function from the simulation were consistent with both the direct measurements and the fits of parametrized models.

Finally, we concluded from our experiments with simulations that our models were still not complex enough to model the small-scale clustering pattern of dark matter halo catalogues, and we were required to introduce a cut $\sigma > \sigma_{\rm min} \sim 6\,h^{-1}$ Mpc in the fitted range to restrict systematic errors in the derived growth rate to a maximum of $\Delta f \approx 0.05$.

4 RESULTS

4.1 Fitting procedure

We fitted the models described in Section 3 to the WiggleZ data set by minimizing the χ^2 statistic calculated as

$$\chi^2 = \sum_{ij} (M_i - D_i)^T C_{ij}^{-1} (M_j - D_j), \tag{15}$$

where M_i is the model vector for i data bins, D_i is the data vector and C_{ij}^{-1} is the element of the inverse covariance matrix which relates bins i and j. Our default redshift–space QCF model contained six parameters $[r_0,\ \gamma,\ q,\ \beta,\ \sigma_v,\ x]$ and we considered variations as described in the text. We used a Monte Carlo Markov Chain (MCMC) code to perform these fits, determining the best-fitting values and joint likelihood distributions of each parameter. We found that chains of 100 000 iterations gave robust results for all models. We double-checked our results using downhill simplex algorithms. Following Contreras et al. (2013), we investigated the dependence of our results on the minimum transverse scale σ included in our fits. The correlation function at low σ may contain the signature of strong non-linearities not fully described by our models, potentially introducing a systematic error in the growth measurement.

4.2 Measurements of the redshift–space distortion parameter β

In Fig. 2 we illustrate the measurements of β in each redshift slice, combining results from the different WiggleZ regions as a function of the minimum transverse separation $\sigma_{\rm min}$. We show results for each of the three real–space correlation-function models introduced above. We found signatures of systematic errors at small scales with the same pattern as found in our investigation of mock halo catalogues from N-body simulations, especially when the power-law model was assumed.

4.3 Measurements of the galaxy bias factor b

We determined the linear galaxy bias factor b, which should be combined with the measurement of β to produce the growth rate $f = \beta\, b$, assuming the CAMB correlation-function model describes well the dark matter correlation function $\xi_{\rm m}$. Then, the bias is determined simultaneously with the other parameters when fitting the CAMB

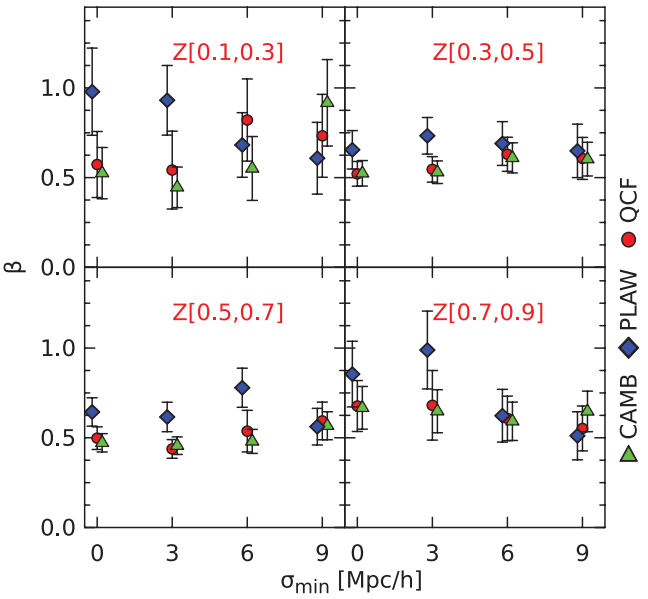

Figure 2. Measurements of the redshift–space distortion parameter β for the four WiggleZ redshift slices, fitting to the combined correlation function of the survey regions. We show results for the three real–space correlation-function models discussed in the text: QCF, CAMB and power law, as a function of the minimum transverse scale $\sigma_{\rm min}$ included in the fit. Note the convergence of the three correlation-function models after small-scale bins are excluded from the fits.

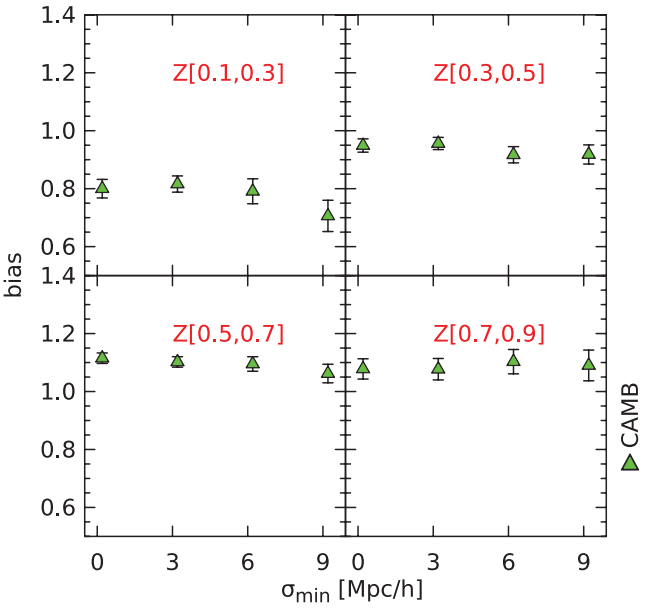

Figure 3. Measurements of the galaxy bias factor in the four WiggleZ redshift slices as a function of the minimum transverse scale $\sigma_{\rm min}$ included in the fit. The bias is determined by fitting a CAMB model to the 2D correlation function. We note that the bias measurements presented in this figure have not been corrected for the effect of redshift blunders (see text).

model to the galaxy correlation function $\xi_{\rm g}$ using

$$\xi_{\rm g} = b^2\, \xi_{\rm m}. \tag{16}$$

Fig. 3 illustrates the best-fitting bias in each redshift slice as a function of $\sigma_{\rm min}$.

The results for x and σ_v show similar behaviour as found in our simulation study: for small $\sigma_{\rm min}$ the value of x favoured an

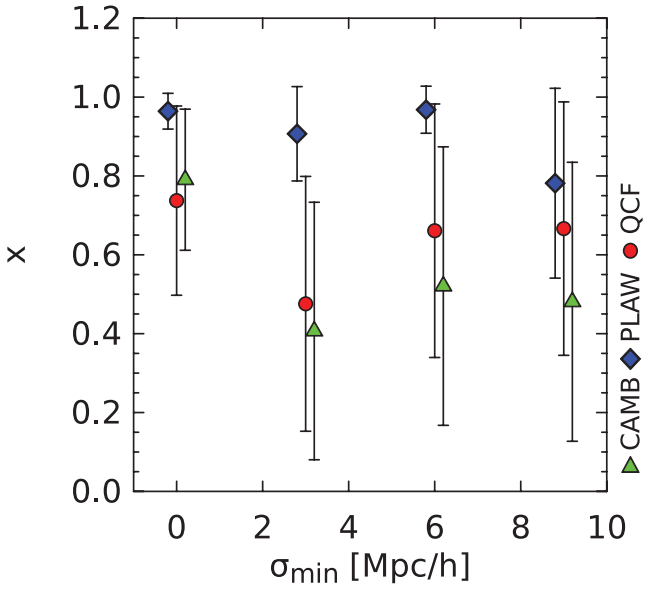

Figure 4. Example of the behaviour of the parameter x as a function of the minimum transverse scale $\sigma_{\rm min}$ included in the fit. Values of x close to 1 implies that $F(v)$ has an exponential shape rather than a Gaussian shape. It becomes less well determined when excluding the small-scale part of the data.

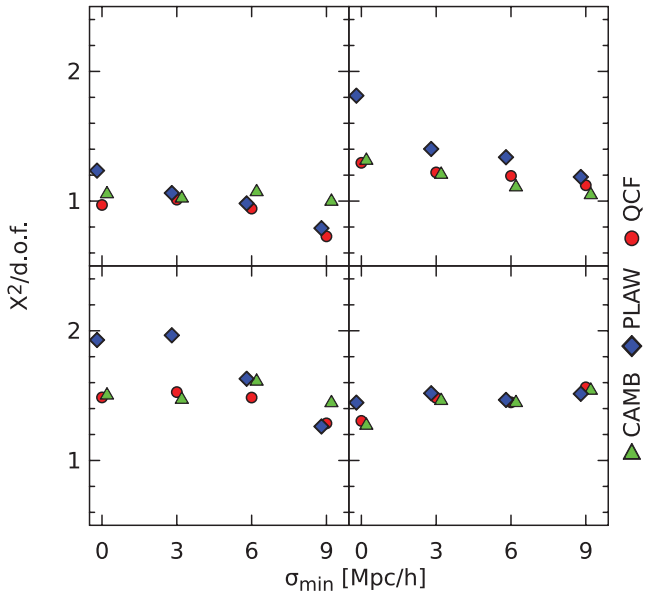

Figure 5. Reduced χ^2 values corresponding to the best-fitting parameters of each of the correlation-function models in the four WiggleZ redshift slices as a function of the minimum transverse scale.

exponential shape for $F(v)$ and σ_v was tightly constrained, and for larger $\sigma_{\rm min}$ both parameters were not well-determined. See Fig. 4 for an example.

The reduced χ^2 values of the best-fitting models are displayed in Fig. 5. We note that the QCF and CAMB models both produce good fits to the data, with the QCF model carrying the additional advantage of not assuming a small-scale shape for the correlation function.

The fitted galaxy bias factors must be corrected for the (relatively small) effects of redshift blunders caused by the mis-identification of emission lines in the WiggleZ survey scattering the true position of galaxies. This effect has been carefully quantified by Blake et al. (2010, section 3.4) and causes a loss of signal in the correlation function which may be recovered by multiplying by a redshift-dependent correction factor:

$$\xi(s)_{\rm corr} = \xi(s)\,[1 - r(z)]^{-2} \qquad (17)$$

where r is the fraction of redshift blunders at redshift z. The relevant correction factors $(1 - r)^{-2}$ for the different redshift slices can be found in Table 2, and are equivalent to an upward correction in the measured galaxy bias factors.

4.4 Stepwise velocity distribution

Our stepwise fitting technique allows us to measure the pairwise velocity distribution in a non-parametric fashion, instead of fixing its shape to some functional form. The 2D correlation function of WiggleZ galaxies does not contain strong 'fingers-of-god' features such as those encountered in redder galaxy samples such as SDSS LRGs. This is expected, as WiggleZ galaxies are blue star-forming galaxies, which inhabit less dense environments than their red counterparts and are thereby less affected by non-linear clustering. Fig. 6 shows the non-parametric stepwise velocity distribution obtained in every redshift slice of our sample. We used seven bins in velocity of width $\sim$300 km s^{-1} up to a maximum of 2000 km s^{-1}. We find a slow growth in the width of the pairwise velocity distribution as redshift decreases, as expected due to the growth of non-linear structure with time. Where the data permit us to discriminate, the measured stepwise distribution is consistent with an exponential function for $F(v)$.

4.5 Measurements of the growth rate f

The final growth rate measurements are obtained by combining β and the bias: $f(z) = \beta\, b$. However, as the bias was measured assuming a CAMB matter correlation function with a fixed normalization σ_8, the measured value of b is degenerate with σ_8. We can convert our measurements to be independent of this effect by quoting the value of $f(z)\sigma_8(z)$ (Song & Percival 2009). In Fig. 7 we display these results in the four redshift slices for different choices of the fitting range $\sigma_{\rm min}$. Motivated by the simulation results presented by Contreras et al. (2013), we take as our preferred measurement the QCF model with $\sigma_{\rm min} = 6\,h^{-1}$ Mpc.

In Fig. 8 we compare these preferred measurements to the results from the analysis of the 2D WiggleZ survey power spectra (Blake et al. 2011a), together with some previous galaxy surveys, and overplot the prediction of a ΛCDM model with matter density $\Omega_{\rm m} = 0.27$ and two different values of the low-redshift normalization $\sigma_8 = 0.7$ and 0.8. The separate measurements using different data sets and techniques are consistent within the statistical errors. The errors in the growth rate measurements using the 2D WiggleZ correlation function are around twice the size of those determined by fits to the power spectra (Blake et al. 2011a). We attribute this to a combination of the greater number of parameters that must be varied to obtain a good fit to the correlation function given the greater relative importance of the non-linear effects that must be modelled, and the more limited range of scales $(\sigma, \pi) < 30\,h^{-1}$ Mpc studied. Nonetheless, the statistical agreement of these analyses is evidence that the different measurements of the growth rate are not dominated by systematic errors.

Table 2. The best-fitting values and errors for the most important parameters of the redshift–space distortion models fitted in each WiggleZ redshift slice.

Redshift slice	$\sigma_{\rm min}$ (h^{-1} Mpc)	QCF model β (Δ_β)	χ^2/dof	CAMB model β (Δ_β)	χ^2/dof	Power-law model β (Δ_β)	χ^2/dof	Bias b (Δ_b)	$\sigma_8(z)$	z-blunder corr.	QCF $f\sigma_8$	CAMB $f\sigma_8$	PLAW $f\sigma_8$
	00	0.57(0.18)	0.970	0.53(0.14)	1.055	0.98(0.24)	1.235	0.80(0.03)			0.36(0.11)	0.33(0.09)	0.61(0.15)
1	03	0.54(0.22)	1.011	0.45(0.11)	1.022	0.93(0.19)	1.062	0.82(0.03)	0.728	1.067	0.34(0.14)	0.28(0.07)	0.59(0.12)
	06	0.82(0.23)	0.942	0.55(0.18)	1.071	0.68(0.18)	0.982	0.79(0.04)			0.50(0.14)	0.34(0.11)	0.42(0.11)
	09	0.73(0.23)	0.728	0.92(0.24)	0.997	0.61(0.20)	0.791	0.71(0.05)			0.40(0.13)	0.50(0.14)	0.33(0.11)
	00	0.52(0.07)	1.295	0.52(0.07)	1.313	0.66(0.11)	1.813	0.95(0.02)			0.34(0.05)	0.35(0.05)	0.43(0.07)
2	03	0.55(0.07)	1.221	0.53(0.06)	1.205	0.73(0.10)	1.402	0.96(0.02)	0.662	1.050	0.36(0.05)	0.35(0.04)	0.49(0.07)
	06	0.63(0.10)	1.194	0.61(0.08)	1.108	0.69(0.12)	1.338	0.92(0.03)			0.40(0.06)	0.39(0.05)	0.44(0.08)
	09	0.61(0.12)	1.122	0.60(0.09)	1.048	0.65(0.15)	1.186	0.92(0.03)			0.39(0.08)	0.38(0.06)	0.41(0.10)
	00	0.50(0.06)	1.486	0.47(0.05)	1.503	0.64(0.08)	1.929	1.11(0.02)			0.35(0.04)	0.33(0.04)	0.46(0.06)
3	03	0.44(0.05)	1.527	0.46(0.05)	1.470	0.62(0.08)	1.965	1.10(0.02)	0.595	1.064	0.31(0.04)	0.32(0.03)	0.43(0.06)
	06	0.54(0.12)	1.485	0.48(0.07)	1.610	0.78(0.11)	1.630	1.09(0.03)			0.37(0.08)	0.33(0.05)	0.54(0.08)
	09	0.59(0.10)	1.286	0.57(0.08)	1.444	0.56(0.10)	1.262	1.06(0.03)			0.40(0.07)	0.38(0.05)	0.38(0.07)
	00	0.68(0.14)	1.305	0.67(0.12)	1.270	0.85(0.18)	1.446	1.08(0.04)			0.46(0.10)	0.46(0.08)	0.58(0.13)
4	03	0.68(0.19)	1.483	0.65(0.12)	1.461	0.99(0.22)	1.518	1.08(0.04)	0.553	1.145	0.46(0.13)	0.44(0.08)	0.67(0.15)
	06	0.61(0.12)	1.448	0.59(0.11)	1.445	0.62(0.15)	1.467	1.10(0.04)			0.42(0.09)	0.41(0.08)	0.44(0.10)
	09	0.55(0.12)	1.564	0.65(0.11)	1.540	0.51(0.13)	1.514	1.09(0.05)			0.38(0.09)	0.45(0.08)	0.35(0.09)

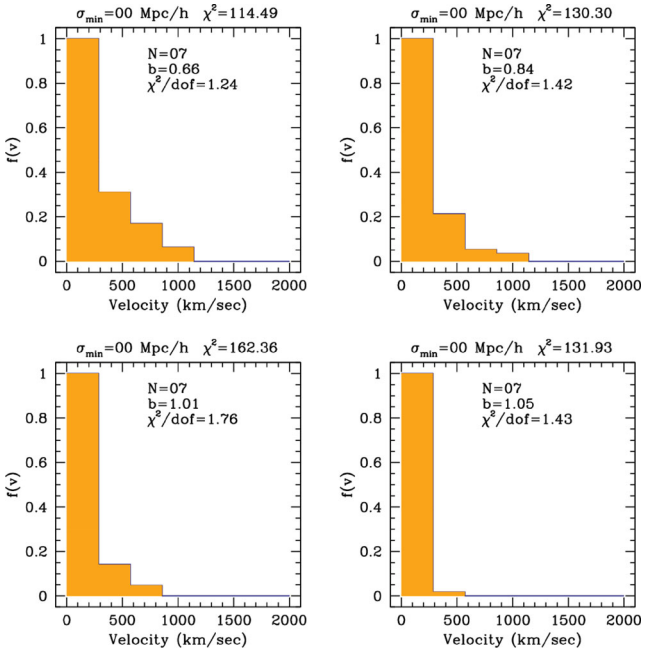

Figure 6. The best-fitting stepwise values of the pairwise velocity distribution of WiggleZ galaxies. We find that the amplitude of the pairwise velocities systematically decreases with increasing redshift, which is expected in a model where non-linear structure grows with time.

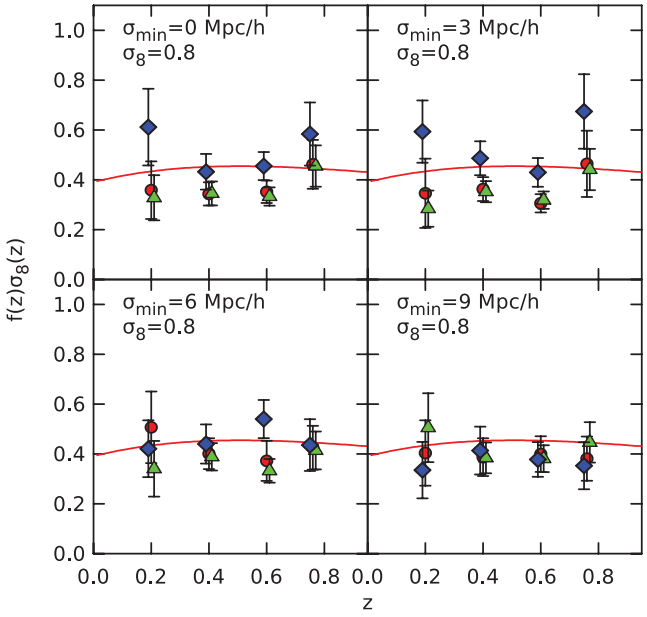

Figure 7. The red circles, green triangles and blue diamonds represent the fitted values of the growth rate in the four WiggleZ redshift slices using a QCF, CAMB and power-law model, respectively, for different data cuts $\sigma > \sigma_{\rm min}$. This plot shows the convergence of the three models when more of the small-scale part of the data is excluded. We note that our simulation study (Contreras et al. 2013) shows that the growth rate is systematically underestimated if $\sigma_{\rm min}$ is too low, with $\sigma_{\rm min} \sim 6\,h^{-1}$ Mpc required to obtain systematic-free results with the QCF model. In all panels we overplot the prediction of a fiducial ΛCDM model with $\Omega_{\rm m} = 0.27$ and $\sigma_8 = 0.8$.

4.6 Effects of the Alcock–Paczynski distortion

Finally we tested the sensitivity of our results to the fiducial cosmological model adopted in our analysis by varying the value of the matter density $\Omega_{\rm m}$. The sensitivity of our measurements to the fiducial model is a result of the Alcock–Paczynski effect (Alcock & Paczynski 1979), a geometrical distortion of the measured clustering pattern which arises if the trial cosmology differs from the true cosmology. The effect is partially degenerate with redshift–space distortions (Ballinger, Peacock & Heavens 1996; Matsubara & Suto 1996; Matsubara 2000; Seo & Eisenstein 2003; Simpson & Peacock 2010) resulting in systematic variations in the best-fitting growth rate as the fiducial cosmology is altered. Alternatively, assuming that the cosmological model is known from a ΛCDM standard gravity model with parameters tuned to match the cosmic microwave background anisotropies, the Alcock–Paczynski effect provides a further cross-check of this model.

We implemented this analysis by repeating our fitting procedure for different values of the fiducial matter density $\Omega_{\rm m} = (0.07, 0.17, 0.37, 0.47)$ for the central redshift slice $z = 0.6$. The results are shown in Fig. 9, demonstrating that the ΛCDM *WMAP*-cosmological model is self-consistent in the range $0.2 < \Omega_{\rm m} < 0.3$

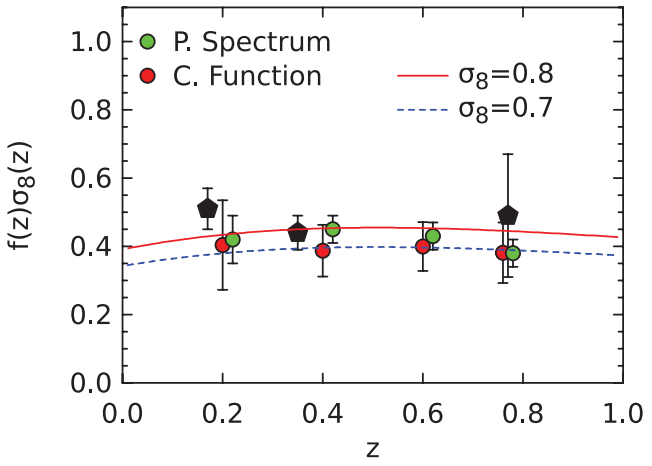

Figure 8. Growth rate results from power-spectrum and correlation-function analyses (green and red circles) of WiggleZ data. In black, we overplot results from the 2dFGRS, SDSS and VVDS surveys (in increasing redshift order). Both WiggleZ sets of results are shifted in redshift for clarity. We show predictions for ΛCDM cosmological models assuming $\Omega_m = 0.27$ and $\sigma_8 = 0.7$ (dashed line) and 0.8 (solid line).

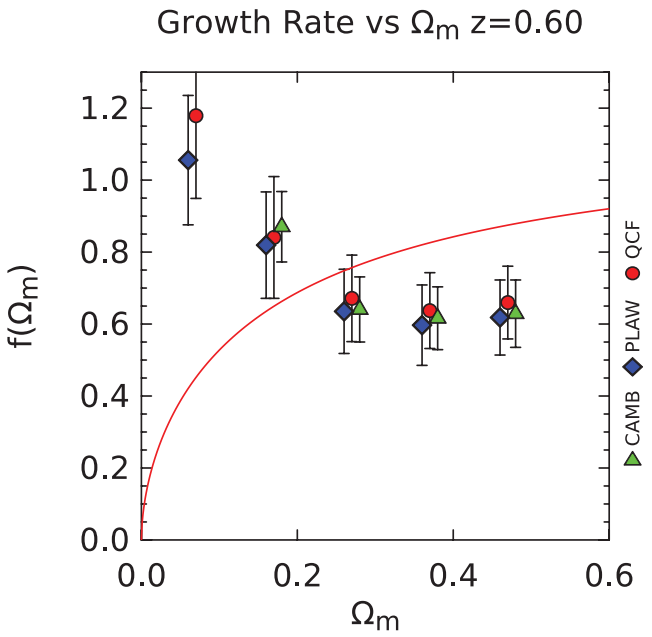

Figure 9. A self-consistency test of the ΛCDM cosmology assuming standard gravity, in which the WiggleZ growth rate measurements in the $z = 0.6$ redshift slice are repeated for different fiducial choices of Ω_m. The results are sensitive to the Alcock–Paczynski effect, and produce a measured growth rate inconsistent with the prediction of standard gravity for both low and high values of Ω_m.

and produces inconsistent results (in standard gravity) for other values of Ω_m. We note, however, that our treatment here is approximate; in our power spectrum model we have fixed the values of the other cosmological parameters at the *WMAP*7 best-fitting values. A full treatment of these model fits is beyond the scope of the current study and is provided by Parkinson et al. (2012).

5 CONCLUSIONS

We have analysed redshift–space distortions in the two-point galaxy correlation function of the WiggleZ Dark Energy Survey built from over 160 000 galaxies, dividing the data set into four redshift slices. We fitted a series of different models to the observed $\xi_s(\sigma, \pi)$ (2D two-point correlation function) using an MCMC process. We summarize our results as follows.

(i) We determine the cosmic growth rate across the redshift range $0.1 < z < 0.9$ with an accuracy of around 20 per cent in each redshift slice of width $\Delta z = 0.2$, and our measurements are consistent with the prediction of a ΛCDM model with $\Omega_m \approx 0.27$ and $\sigma_8 \approx 0.8$.

(ii) Our results are also consistent with an independent power-spectrum analysis of a similar data set (Blake et al. 2011b), demonstrating that systematic errors are not significant in these two different approaches.

(iii) We perform a non-parametric determination of the pairwise velocity distribution of WiggleZ galaxies as a stepwise function, demonstrating that the amplitude of pairwise velocities grows with decreasing redshift, as expected due to the growth of non-linear structure with time, and that (where it is possible to fit a model) it is well-described by an exponential function.

(iv) Our measurements agree well with the behaviour found in our previous experiments using *N*-body simulations (Contreras et al. 2013), and we obtain a convergence in the different models for the growth rate when excluding the small-scale non-linear part of the data ($\sigma < 6\,h^{-1}$ Mpc).

(v) We repeated the entire procedure (from transforming redshift catalogues into 3D spatial galaxy distributions to running MCMC correlation-function model-fitting) for ΛCDM cosmologies with different values of Ω_m. The results show that the ΛCDM model is only self-consistent in the range $0.2 < \Omega_m < 0.3$.

We conclude that the standard ΛCDM cosmological model provides a good description of the growth rate which drives redshift–space distortions in the clustering of WiggleZ galaxies, using cosmological parameters which also yield a good simultaneous fit to the expansion history measured by baryon acoustic oscillations and supernovae, and to the fluctuations in the cosmic microwave background radiation. We have shown that different statistical analyses of the WiggleZ data set, with very different potential systematic errors, produce growth rate measurements in close mutual agreement.

ACKNOWLEDGMENTS

We acknowledge financial support from the Australian Research Council through Discovery Project grants which have funded the positions of MP, GP, TD and FM. SMC acknowledges the support of the Australian Research Council through a QEII Fellowship. MJD and TD thank the Gregg Thompson Dark Energy Travel Fund for financial support. CC thanks David Parkinson for sharing his expertise on MCMC techniques, and Ana María Martínez for her invaluable feedback and support in the building of this paper.

GALEX is a NASA Small Explorer, launched in 2003 April. We gratefully acknowledge NASA's support for construction, operation and science analysis for the *GALEX* mission, developed in co-operation with the Centre National d'Etudes Spatiales of France and the Korean Ministry of Science and Technology.

Finally, the WiggleZ survey would not have been possible without the dedicated work of the staff of the Australian Astronomical Observatory in the development and support of the AAOmega spectrograph, and the running of the AAT.

This research was supported by CAASTRO: http://caastro.org.

REFERENCES

Abate A., Lahav O., 2008, MNRAS, 389, L47
Alcock C., Paczynski B., 1979, Nat, 281, 358
Ballinger W., Peacock J., Heavens A., 1996, MNRAS, 282, 877
Bernstein G., 2009, ApJ, 695, 652
Blake C. et al., 2009, MNRAS, 395, 240
Blake C. et al., 2010, MNRAS, 406, 803
Blake C. et al., 2011a, MNRAS, 415, 2876
Blake C. et al., 2011b, MNRAS, 418, 1707
Cabré A., Gaztañaga E., 2009, MNRAS, 396, 1119
Colless M. et al., 2001, MNRAS, 328, 1039
Contreras C., Blake C., Poole G., Marin F., 2013, MNRAS, submitted
da Angela J. et al., 2008, MNRAS, 383, 565
Drinkwater M. J. et al., 2010, MNRAS, 401, 1429
Guzzo L. et al., 2008, Nat, 451, 541
Hamilton A. J. S., 1992, ApJ, 385, L5
Hamilton A. J. S., 1993, ApJ, 417, 19
Hawkins E. et al., 2003, MNRAS, 346, 78
Heavens A. F., Kitching T. D., Verde L., 2007, MNRAS, 380, 1029
Kaiser N., 1987, MNRAS, 227, 1
Landy S. D., Szalay A. S., 1993, ApJ, 412, 64
Landy S., Szalay A., 1998, ApJ, 494, L133
Lewis A., Challinor A., Lasenby A., 2000, ApJ, 538, 473
Linder E., Cahn R., 2007, Astropart. Phys., 28, 481
Linder E., Jenkins A., 2003, MNRAS, 346, 573
Matsubara T., 2000, ApJ, 535, 1
Matsubara T., Suto Y., 1996, ApJ, 470, L1
Nusser A., Davis M., 2011, ApJ, 736, 93
Okumura T., Matsubara T., Eisenstein D. J., Kayo I., Hikage C., Szalay A. S., Schneider D. P., 2008, ApJ, 676, 889
Parkinson D. et al., 2012, Phys. Rev. D, 86, 103518
Peebles P. J. E., 1980, The Large-Scale Structure of the Universe. Princeton Univ. Press, Princeton, NJ
Percival W. et al., 2004, MNRAS, 353, 1201
Rapetti D., Allen S., Mantz A., Ebeling H., 2009, MNRAS, 400, 699
Samushia L., Percival W. J., Raccanelli A., 2012, MNRAS, 420, 2102
Seo H.-J., Eisenstein D., 2003, ApJ, 598, 720
Simpson F., Peacock J., 2010, Phys. Rev. D, 81, 043512
Song Y.-S., Percival W. J., 2009, J. Cosmol. Astropart. Phys., 004
Tegmark M. et al., 2006, Phys. Rev. D, 74, 123507
Tsujikawa S., 2010, preprint (arXiv:1004.1493v1)
Wang Y., 2008, J. Cosmol. Astropart. Phys., 05, 021
Watkins R., Feldman H. A., Hudson M. J., 2009, MNRAS, 392, 7430
Yee H., Hsieh B., Lin H., Gladders M., 2005, ApJ, 629, L77
York D. et al., 2000, AJ, 120, 1579

This paper has been typeset from a TEX/LATEX file prepared by the author.